RSC Pharmaceutics

ROYAL SOCIETY OF CHEMISTRY

PAPER

View Article Online
View Journal | View Issue

Cite this: *RSC Pharm.*, 2025, **2**, 82

On-demand release of encapsulated ZnO nanoparticles and chemotherapeutics for drug delivery applications†

Josh E. Eixenberger, *[a,b] Catherine B. Anders,[a] Rebecca Hermann,[d] Katelyn Wada,[b] Kongara M. Reddy,[b] Raquel J. Montenegro-Brown,[c] Daniel Fologea[a,b] and Denise G. Wingett *[a,d]

Nanomedicines offer high promise for the treatment of various diseases, and numerous novel approaches using nanomaterials have been developed over the years. In this report, we introduce a new strategy utilizing ZnO nanoparticles (nZnO) to trigger the rapid release of lipid-encapsulated therapeutics upon photo-irradiation with UV light (365 nm). *In vitro* studies demonstrate that encapsulation of nZnO effectively eliminates the cytotoxicity of nZnO, but this can be re-established upon release from the lipid coating. Using 5(6)-carboxyfluorescein as a model for hydrophilic drug loading, we show the ability to co-load drugs with nZnO into liposomes. Kinetic studies reveal the ability to release the majority of the dye within 60 minutes post-photo-irradiation and provide insights into factors that impact release kinetics. To further explore this, Jurkat T cell leukemia and T47D breast cancer cells were treated with co-encapsulated nZnO and the hydrophobic cancer drug paclitaxel. These studies revealed enhanced toxicity of the triggered release groups with an extreme difference noted in the viability profiles of the T47D breast cancer cell model. Taken together, these studies indicate that this system of co-encapsulating nZnO and chemotherapeutic drugs has the potential to minimize systemic toxicity, by controlling therapeutic release, while allowing for the localized selective destruction of cancer.

Received 28th June 2024,
Accepted 17th October 2024

DOI: 10.1039/d4pm00189c

rsc.li/RSCPharma

Introduction

Over the last few decades, tremendous strides have been made in combatting cancer; however, it is estimated that ~10 million cancer-related deaths still occur yearly, worldwide.[1] While there have been a number of new successful therapeutic options developed, such as immunotherapy, most therapies still employ conventional methods, namely, radiation therapy, chemotherapy, and surgery.[2] Unfortunately, these therapeutic options and more specifically chemotherapeutics suffer from a large number of side effects.[3] One potential avenue to reduce or eliminate side effects is to limit systemic exposure of chemotherapeutics, while still achieving the required dose to cancerous cells. There have been numerous targeting strategies that aim to realize this goal, with novel nanotechnology-based therapies being heralded as a potential solution.

Nanobiotechnology is a rapidly growing field with numerous applications geared towards biomedical purposes. Nanomedicines are being used in the treatment, diagnosis, and prevention of diseases, where many novel nanostructures offer considerable promise. Currently, there are already over 50 FDA-approved nanomedicines, and numerous others are in clinical trials.[4] The goal of many of these new technologies is to either improve upon already existing technologies or offer new therapeutic treatment options that increase efficacy and minimize off-target side effects. Towards this aim, ZnO nanoparticles (nZnO) have been utilized in various potential drug delivery devices,[5] and have many intrinsic features that make them good candidates for therapeutic applications.

One of the well-known physical properties and proposed toxicity mechanisms of nZnO is particle dissolution. This feature is enhanced in lower pH environments, such as in certain tumors or intracellular compartments, and has been exploited as a means to control drug release. An example of utilizing the dissolution potential of ZnO is to encapsulate doxorubicin-loaded SiO_2 nanoparticles (NPs) with a layer of

[a]*Biomolecular Sciences Graduate Program, Boise State University, Boise, ID 83725, USA. E-mail: JoshEixenberger@boisestate.edu; Tel: +208-426-2231*
[b]*Department of Physics, Boise State University, Boise, ID 83725, USA*
[c]*Biomolecular Research Center, Boise State University, Boise, ID 83725, USA*
[d]*Department of Biological Sciences, Boise State University, Boise, ID 83725, USA. E-mail: DeniseWingett@boisestate.edu; Tel: +208-426-2921*

† Electronic supplementary information (ESI) available. See DOI: https://doi.org/10.1039/d4pm00189c

ZnO.[6] The ZnO layer prevents premature drug leakage, yet when exposed to a lower pH, the quick dissolution of ZnO induces the release of the drug.

In addition to their high dissolution potential, nZnO and many other metal oxide NPs have strong photocatalytic activity, which is a property that can also be exploited for use in potential therapeutics. Photo-irradiation of these semiconductor NPs induces the generation of reactive oxygen species (ROS) which can be utilized for various purposes.[7,8] nZnO, in particular, exhibits increased toxicity towards cancer cells when exposed to UV light.[9,10] Phototherapy treatment experiments with nZnO confirm increased ROS generation that can lead to extensive lipid peroxidation of cellular membranes.[11–13] Since the peroxidation of lipids can lead to lipid radicals that propagate throughout the bilayer, this process can lead to the rupture of cellular membranes.[14,15] Collectively, the physicochemical properties of nZnO have led to the development of novel strategies to combat diseases and highlight why numerous researchers are pursuing its use as a therapeutic.

nZnO also exhibits inherent selective toxicity towards various cancer types when compared with the normal non-malignant cell types of identical lineage.[15–17] Studies have even reported up to a 33-fold higher selectivity towards cancerous cells, a higher therapeutic index than those of many traditionally used chemotherapeutics using similar assays.[18] Importantly, the selective nature of nZnO for cancers, such as squamous cell lung cancer and pancreatic adenocarcinoma, has been demonstrated in mouse models and is not just a novelty of *in vitro* experiments.[19,20] While nZnO structures have been used for potential therapeutic purposes, research suggests that nZnO may be utilized in diagnostics, such as MRI, CT, and bio-imaging applications.[20–22]

Even though there have been numerous strategies that utilize nZnO for therapeutic applications, there do still exist some limitations to its use. With the high dissolution potential of nZnO, its introduction into biological fluids can induce the dissolution of the particles before they reach their target site.[23–26] Furthermore, nZnO is prone to agglomeration, especially in environments with high ionic concentrations such as in biological fluids.[27,28] Early dissolution and agglomeration may impede the effectiveness of nZnO as a therapeutic and thus, many studies have looked at ways to achieve a more stable nZnO suspension. A common strategy to stabilize nZnO in solution is to coat the particles with polymers or biomolecules.[27,29] Since lipid vesicles are already extensively used for drug delivery, coating nZnO with lipids may increase the stability of nZnO while simultaneously preventing premature dissolution.

Hybrid liposome–inorganic NPs offer an interesting avenue for drug delivery, and liposomal formulations already make up a large fraction of the currently FDA-approved nanomedicines.[4] The attributes that make lipids attractive for drug delivery include high biocompatibility, ease of synthesis, targeting by both active and passive processes, and various means of controlling drug release.[4,30,31] Since lipids are amphipathic, both hydrophobic and hydrophilic drugs can be loaded within liposomes, a feature that has enabled their use in both approved nanomedicines and those undergoing clinical trials. Many formulations of liposomes have high encapsulation efficiency for both hydrophobic and hydrophilic drugs which can improve drug stability and pharmacokinetics. However, unmodified liposomes themselves are recognized by the immune system and are quickly cleared from circulation.[32] This drawback has been overcome by the creation of "stealth" liposomes. For example, the conjugation of polyethylene glycol (PEG) to the head group of lipids prevents the reticuloendothelial system from rapidly clearing the stealth liposomes and increases circulation time.[4,32,33]

Liposomes can be further modified for active targeting strategies in which ligands or antibodies, specific for individual cell surface receptors, can be conjugated to the surface of the liposome. This approach can improve liposomal localization in tissues that overexpress these surface receptors. Passive targeting has been another avenue that researchers have pursued, as NPs in the size range of 4–200 nm can accumulate in tumor environments that have a "leaky" vasculature and avoid clearance due to reduced local lymphatic drainage. This feature is termed the enhanced permeability and retention (EPR) effect and is present in certain tumor morphologies.[34,35] Targeting capabilities offer the promise of improved efficacy by high concentrations of the drug being released in the target area and can simultaneously reduce the amount of overall drug concentration needed in hopes of reducing or eliminating unwanted side effects.

Controlled release of liposomal contents has been achieved through various mechanisms. For example, pH sensitive lipids such as dioleoylphosphatidylethanolamine (DOPE) allow for increased membrane permeability when incorporated into the bilayer and subsequently exposed to a lower pH environment.[36,37] As many tumor microenvironments have a relatively acidic pH, this approach has been pursued as a means to release high payloads of drugs in a localized area.

With a variety of nanotechnologies currently under development, there is significant hope for improved drug delivery and diagnostic options that allow for increased patient survival while minimizing the side effects commonly associated with current chemotherapeutics. In this regard, we aim to combine the promising attributes of nZnO and the efficiency of lipid carriers for drug delivery into one therapeutic platform that realizes the benefits of both systems. Here we report on the utilization of the ROS-generating capabilities of nZnO to trigger the rapid release of cargo contained within a lipid carrier as a potential new drug delivery strategy.

Results and discussion

nZnO synthesis and characterization

ZnO nanoparticles (nZnO) were synthesized using a previously reported wet chemical method utilizing DEG as a solvent.[38] This particular synthesis method was employed as it produces essentially pure nZnO with a reduced band gap (~3.1 eV or

400 nm) that allows for the nZnO to be imaged using fluorescence microscopy techniques (405 nm excitation) without modifications to the nZnO. XRD measurements verified phase purity with an average crystal size of 15.1 ± 1.8 nm. TEM images (Fig. S1†) show that the individual nZnO crystals form larger aggregates of 50–400 nm. Dynamic light scattering measurements in nanopure water and 130 mM NaCl yielded an average hydrodynamic size (HDS) of the aggregated nZnO of 317 ± 2.87 nm and 2092 ± 149.4 nm with a polydispersity index (PDI) of 0.122 and 0.4, respectively (Fig. S2† for size distributions). FTIR and XPS were used to confirm that the nZnO was essentially pure with only trace amounts of carbon dioxide and hydroxyl stretching groups (Fig. S3†). Extensive synthesis and characterization details for this nZnO formulation have been previously reported.[38]

Encapsulation, imaging and viability assessments of nZnO

Sonication of lipids above their phase transition temperature has been used to produce single bilayer lipid vesicles and is a common method employed for producing small liposomes.[39,40] In order to encapsulate nZnO, this strategy involved incorporating the nZnO during the sonication procedure using a 130 mM NaCl solution to prevent osmotic pressure effects upon introduction into cellular media. Confocal microscopy was used to evaluate the encapsulation efficiency of the nZnO. As shown in Fig. 1, the fluorescent signal from the lipid membrane stain overlays with the fluorescent nZnO, demonstrating good encapsulation of the nZnO. Additionally, TEM images were obtained of the lipid coated nZnO to further validate the encapsulation. Dynamic light scattering measurements were subsequently performed on Enc-nZnO. A drastic decrease in the HDS was observed, resulting in a size distribution more similar to the free nZnO in nanopure water (739.5 ± 15.5 nm) when compared to the salt solution control (2092 nm) (Fig. S2†). This feature, attributed to the stabilization of the nZnO in the solution, is likely a result of the hydrophilic surface of the lipid encapsulation preventing agglomeration of the nZnO.[41] This stabilization remained consistent over many months and allowed for the Enc-nZnO to be stored and easily dispersed by gentle shaking when used for subsequent experiments.

To determine the impact that encapsulating nZnO has on toxicity, both Jurkat T cell leukemia (suspension) and T47D breast cancer (adherent) cells were treated with both free nZnO and Enc-nZnO for 48 hours. nZnO sedimentation and, more specifically, the tendency of nZnO to agglomerate and become an unstable suspension in cellular media result in both decreased viability of adherent cells and increased viability of suspension cells due to differences in dosimetry.[27,42] Enc-nZnO, with a decreased HDS and a lipid coating, is more biologically stable and has been reported that cells exhibit increased uptake of Enc-nZnO.[43] However, the lipid encapsulation may reduce interactions of the highly reactive nZnO surface with cells and reduce/eliminate its dissolution in cellular media, significantly altering its toxicity profile.

As can be seen in Fig. 2, coating nZnO with lipids in this system effectively eliminated the observed toxicity for both Jurkat and T47D cancer cell types, even when treated with concentrations of up to ~10 times (122.21 μg mL^{-1}) the IC_{50} of the bare nZnO samples (12.86 μg mL^{-1} no UV; 12.2 μg mL^{-1} UV; see ESI Fig. S4† for dose–response curves). Studies also revealed the ability to trigger the release of Enc-nZnO by irradiation with a 365 nm LED UV lamp. Within a few minutes of UV exposure, the lipid barrier was disrupted and the toxic

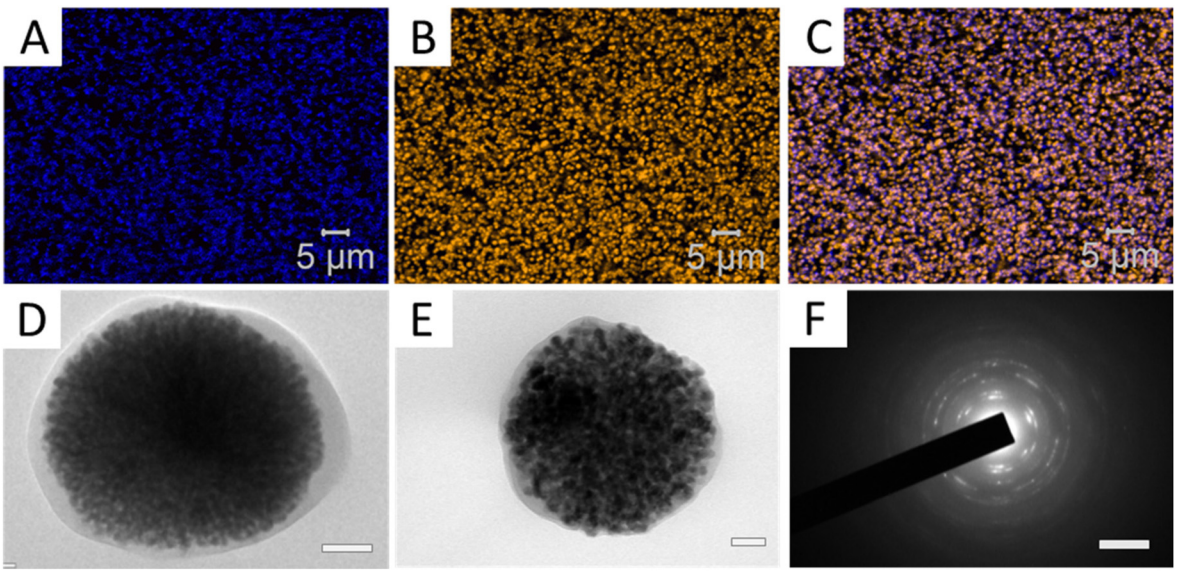

Fig. 1 Confocal microscopy image of (A) fluorescent nZnO, excited by a 405 nm laser, (B) the lipid membrane stained with Cell Mask Orange, and (C) an overlay of (A) and (B), demonstrating efficient encapsulation of nZnO. (D and E) TEM images of the ZnO nanoparticles encapsulated within the lipid coating (D: scale bar = 100 nm; E: scale bar = 50 nm). (F) Electron diffraction pattern of (D) demonstrating that the encapsulated material is ZnO (scale bar = 51 nm).

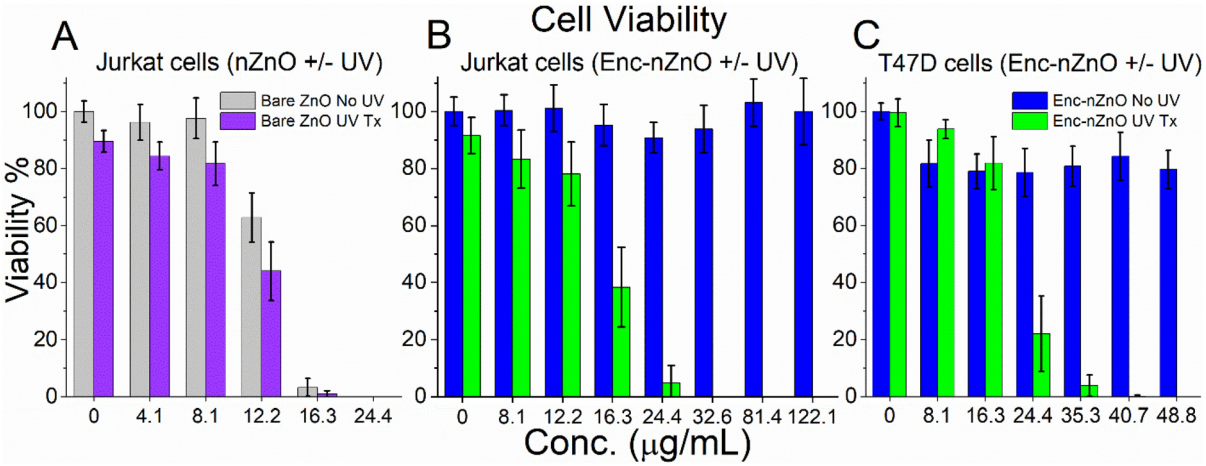

Fig. 2 Viability profiles of (A) Jurkat T cell leukemia treated with free nZnO (non-encapsulated), (B) Jurkat cells treated with Enc-nZnO and (C) T47D breast cancer cells treated with Enc-nZnO for 48 hours. (B and C) The non-UV groups (blue bars) show that the membrane encapsulation of nZnO protects the cells from the toxic effects of the NPs. The UV treatment groups (green bars) demonstrate that the toxic effects of nZnO have been reestablished by the triggered release of the particles, most likely due to ROS generated from nZnO and subsequent shedding of the lipid coating. UV exposure = 3 minutes for Jurkat T cells; 2 minutes for T47D cells.

effect of nZnO on cancer cells became evident across a wide range of concentrations (Fig. 2).

Confocal microscopy was utilized to visualize both the protective effect of encapsulating nZnO and to observe the restored toxic effect of nZnO, once released using the T47D cell line. As can be seen in Fig. 3(D–F), even after 24 hours post-treatment using concentrations of Enc-nZnO that are higher than those used in the T47D viability experiments (80.1 μg mL^{-1}; 1 mM), the lipid coating protected the cells from the toxic effects of nZnO. Notably, the cell confluency is unaffected with little to no nZnO seen within the interior of the cells, even though high concentrations are present near the exterior of the cells. This is in stark contrast to photo-irradiated cells treated with relatively low concentrations of Enc-nZnO (20.3 μg mL^{-1}; 250 μM; Fig. 3(G–I)) where the membrane morphology is compromised, and the stain no longer overlays with the particles as it does in the non-irradiated cell samples (Fig. 3). This observation suggests that Enc-nZnO sheds the lipid coating upon photo-irradiation. It was also noted that in the irradiated group (Fig. 3(G–I)), the cell density is greatly reduced and nZnO appears to have been internalized into the cells. These results confirm the viability profiles and indicate the protective effect that the lipid coating has on the toxicity of nZnO.

Simulated and *in vitro* drug release experiments

Photoirradiation of nZnO with energy higher than the band gap of ZnO can lead to the generation of ROS.[44] The ROS-generating capabilities of nZnO have been proposed to be produced from excited electrons in the conduction band reacting with adsorbed O_2 molecules and locally adsorbed OH– interacting with valence band holes.[44] It is hypothesized that irradiating Enc-nZnO causes nZnO to generate ROS leading to rapid and propagating lipid peroxidation and the subsequent release of both nZnO and any other cargo contained within the lipid carrier. To understand the release kinetics upon photo-irradiation, the fluorescent dye 5(6)-carboxyfluorescein (CF) was used as a hydrophilic drug model and co-encapsulated with nZnO.

Fluorescent dyes are often used in drug release models by encapsulating the dye at self-quenching concentrations. Upon release of the dye, the fluorescence is restored due to the low overall concentration in the solution, which allows for assessments of drug release kinetics and entrapment efficiency (see Fig. S5† for the self-quenching curve).[45–48] Using this established model, we evaluated the effect that the lipid to nZnO ratio has on the release kinetics and premature drug escape. As seen in the non-irradiated samples, the lower lipid to nZnO ratio (3 : 4) resulted in premature dye leakage before irradiation (Fig. 4A), but once irradiated, the release kinetics increased (Fig. 4(B and C); 3 : 4 w/w). Greater lipid to nZnO ratios almost entirely eliminated the premature release of the dye, but even with a reduced release rate, the samples irradiated for both 5 and 15 minutes respectively still achieved similar total amounts of dye release (Fig. 4B and C).

The pH of the solution can impact the ROS-generating capabilities of irradiated nZnO,[44] and therefore, experiments were performed using a higher pH (pH = 9.85) in the interior of the encapsulated nZnO/CF. Fig. 4D demonstrates that the higher pH in the interior of the lipid carrier increased the release kinetics and achieved a higher total release than in any other experiment.

The fluorescent dye was an excellent model for hydrophilic drugs and gave valuable insights into the release kinetics, which revealed how both the ratio of lipids to nZnO and pH can alter the release profiles. To further illustrate the potential of this system to be used as a therapeutic, we co-encapsulated nZnO and the hydrophobic drug paclitaxel. Paclitaxel (PTX) is

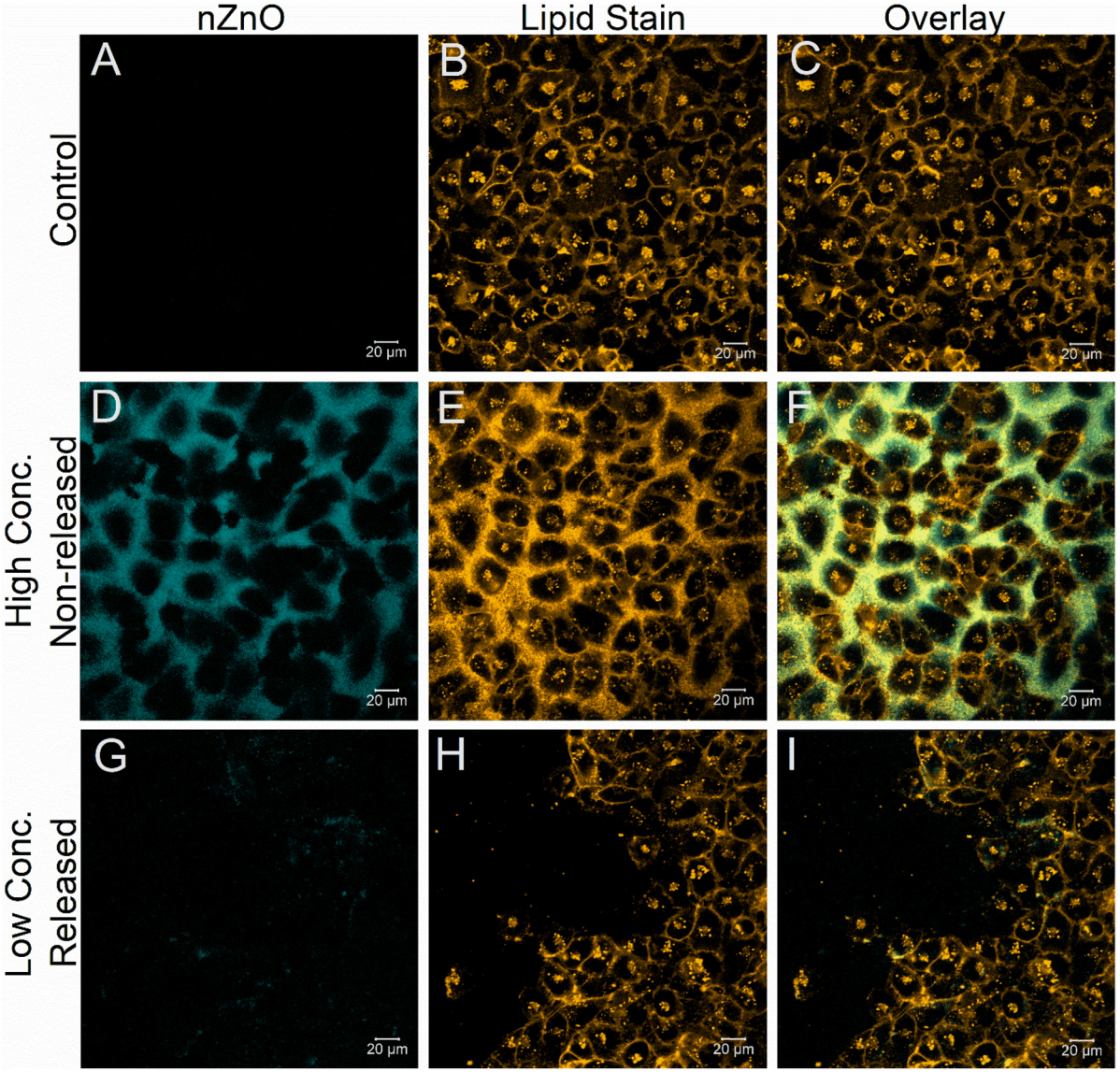

Fig. 3 Confocal images of T47D breast cancer cells after 48 hours of incubation in the imaging chambers and 24 hours post nZnO treatment. The top row (A–C) depicts untreated T47D cells incubated in the absence of nZnO (negative control) illustrating a lack of auto-fluorescence from the cells in the nZnO channel. The lipid membrane stain Cell Mask Orange was utilized to demonstrate the normal morphology of the cells (B). (D–F) T47D cells treated with 81.4 μg mL^{-1} (1 mM) of encapsulated nZnO (Enc-nZnO) 24 hours prior to imaging. These images reveal that even at relatively high concentrations of Enc-nZnO (80.1 μg mL^{-1}), the cell morphology and confluency do not appear to be affected, suggesting that the toxicity of Enc-nZnO is negligible. The bottom row (G–I) of T47D cells treated with 20.3 μg mL^{-1} (250 μM) of Enc-nZnO and irradiated for 2 minutes shows changes in the confluency of the cells and an apparent loss of cell membrane integrity.

commonly used in the treatment of various cancers but due to its high hydrophobicity, it is most often prepared in a formulation with polyoxyethylated castor oil which leads to numerous side effects including hypersensitivity reactions.[49–52] New formulations including protein- and lipid-based nanocarriers have been developed, yet PTX can be reabsorbed by the carrier due to its hydrophobicity which may impede PTX's effectiveness. A more efficient mechanism of delivery could involve using ROS to stimulate the release; ROS generation leads to lipid peroxidation of the hydrophobic lipid tails, resulting in a loss of hydrophobicity which would lead to efficient drug release and prevent reuptake of the drug. In the pursuit to develop this new carrier and release system, we sought to show that both classes of drugs can be co-encapsulated with nZnO and used to treat the Jurkat and T47D cancer cell lines.

Fig. 5 demonstrates that co-encapsulated PTX and nZnO (Enc-nZnO/PTX) can be simultaneously delivered to Jurkat cells within the lipid carrier to exert their toxic effects. In the non-triggered release viability experiments (blue), the Jurkat T cell viability profile was similar to the free PTX treatment (Fig. 5A). While this is consistent with studies that report that lipid carriers for PTX have similar cell viability profiles to

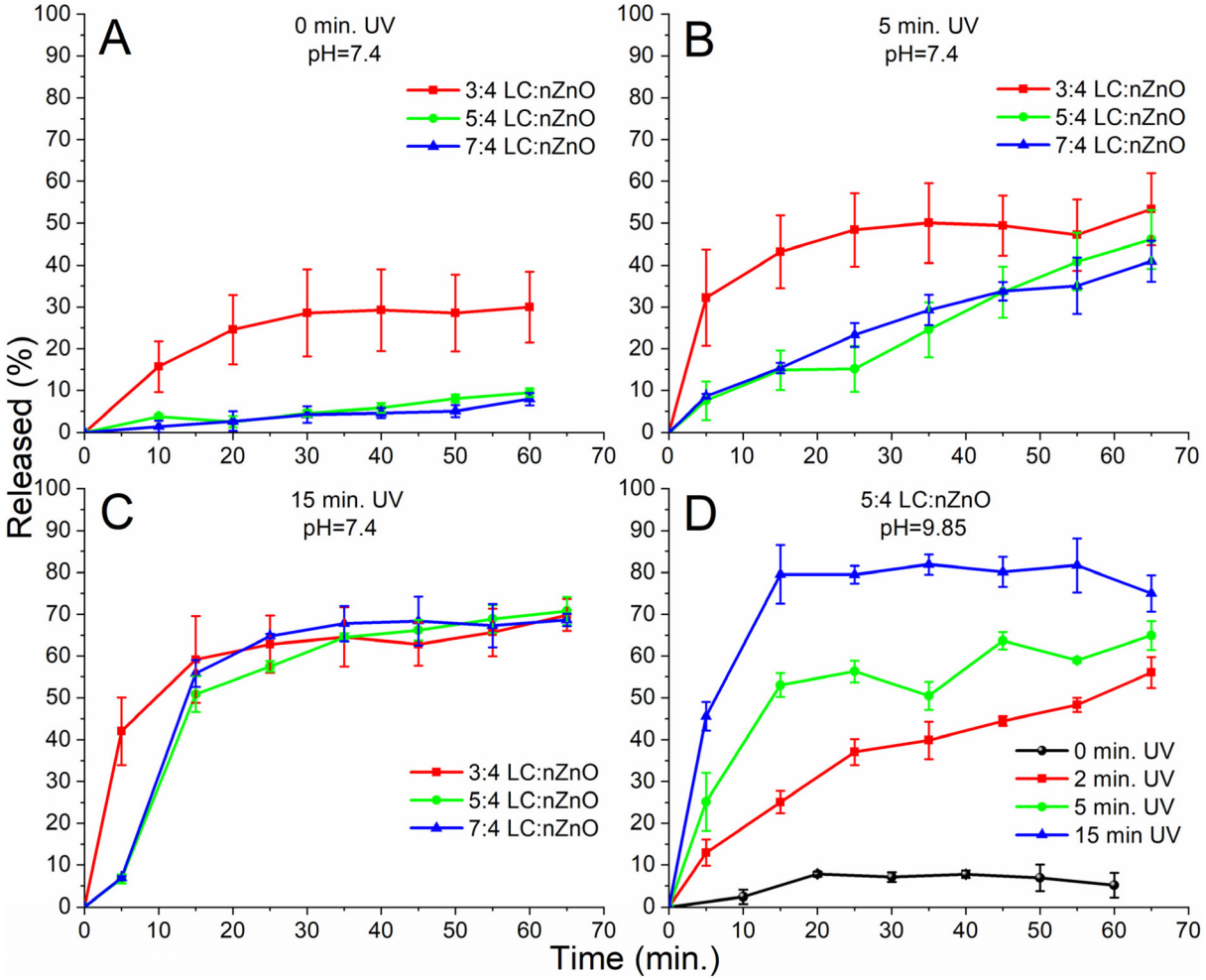

Fig. 4 (A–C) Release kinetics of encapsulated 5(6)-carboxyfluorescein (pH = 7.4) and nZnO with various lipid/chol (LC) to nZnO ratios (w/w); (A) non-triggered release (No UV) group to evaluate premature drug leakage from the different lipid to nZnO ratios; (B) release kinetics after 5 minutes of UV exposure; and (C) release kinetics after 15 minutes of UV exposure. These release profiles demonstrate that the majority of the contents can be rapidly released within 60 minutes and provide insights into the optimal LC to NP ratio. (D) Release kinetics of encapsulated 5(6)-carboxyfluorescein (pH = 9.85) and nZnO encapsulated at a 5 : 4 LC to NP ratio; nZnO in a higher pH environment produces more ROS, thus allowing for a faster release of the dye with less irradiation time.

using "free" PTX,[53,54] the triggered release groups (green) showed a trend of improved efficacy. These initial studies utilized concentrations of both nZnO and PTX that were near the IC_{50} of their free counterparts to evaluate potential additive or synergistic effects, but even though a reduction in viability was seen, synergistic enhancement was not observed.

While simultaneous exposure to both nZnO and PTX could be beneficial for the treatment of cancer, we also wanted to assess the efficacy of this drug delivery system while minimizing the effects of nZnO toxicity. To accomplish this, PTX was loaded at a higher concentration (Fig. 5B), in order to mitigate the direct toxicity effects from nZnO. Interestingly, even with concentrations of nZnO that did not impact the viability of the cells, an increase in toxicity of the triggered release group was still achieved when compared to the free drug (Fig. 5B). These findings demonstrate that the triggered release of PTX from the lipid carrier improves the efficacy of the drug in this system (see Fig. 5C for controls and comparison of the two ratios), but these results are also influenced by decreased viability due to UV irradiation.

To evaluate the impact of this delivery platform on other cancer cell lines, we repeated the experiments with the adherent T47D breast cancer cells. Interestingly, T47D cells revealed extremely different viability profiles when comparing the irradiated groups to the non-released groups (Fig. 6). As the T47D cell line behaved remarkably different from the Jurkat cells, we sought to explain why there was such a striking difference in the viability profiles. Our previous experiments with Enc-nZnO (no PTX; Fig. 2C) showed no appreciable difference in toxicity between the control and the irradiated groups at concentrations of nZnO up to 16.3 μg mL^{-1} (200 μM) and yet close to 40%+ difference in viability was noted in the Enc-nZnO/PTX groups at or above this nZnO concentration (Fig. 6A).

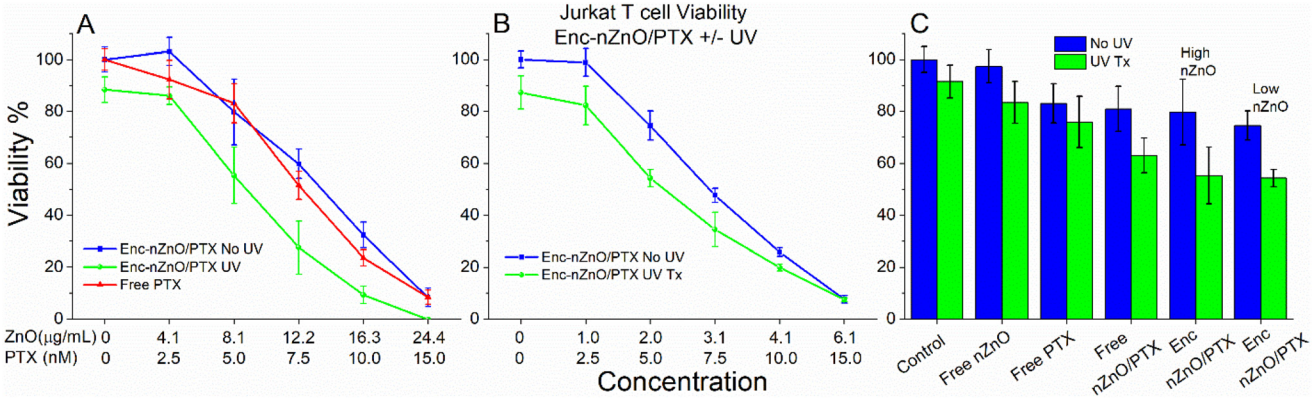

Fig. 5 Viability of Jurkat T cells after 48 hours of treatment with paclitaxel (PTX) co-loaded with Enc-nZnO (Enc-nZnO/PTX) and various controls. (A) The viability profile of the Jurkat cells when treated with free PTX and relatively higher nZnO to PTX ratios. On comparing the released (UV Tx) *vs.* the non-released (No UV) groups, an increase in toxicity is noted for every concentration tested. (B) Relatively lower nZnO to PTX ratios were utilized to demonstrate that increased toxicity is still seen in the triggered release group at concentrations of nZnO that do not impact cell viability when used alone. All treatment concentrations in (A) and (B) have a $p < 0.005$ when comparing the UV *vs.* No UV treatments except for the 6.1 μg mL^{-1}–15 nM treatment in (B) that has $p = 0.8715$ calculated using ANOVA. (C) Treatments with the free drug PTX (5.0 nM), free nZnO (8.1 μg mL^{-1}) and free nZnO/PTX (8.1 μg mL^{-1}–5.0 nM) compared with Enc-nZnO/PTX (high-nZnO 8.1 μg mL^{-1}; low-nZnO 2.0 μg mL^{-1}; both high/low PTX 5.0 nM) with and without UV exposure.

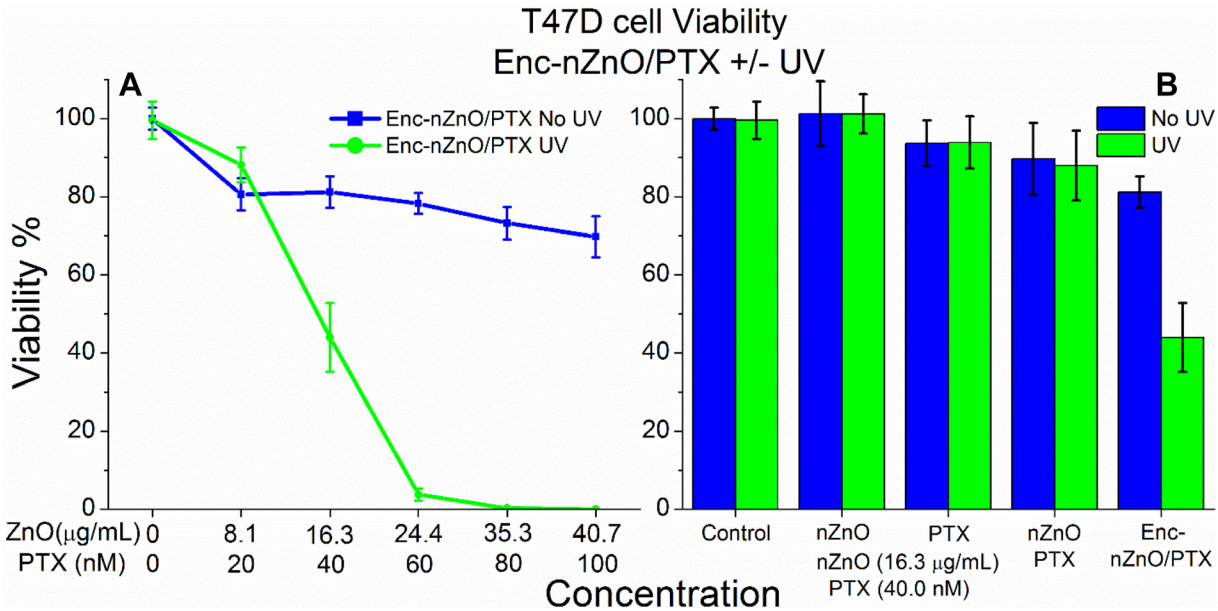

Fig. 6 Viability profile of T47D breast cancer cells after 48 hours of treatment using Enc-nZnO/PTX with and without UV irradiation. (A) The viability profile of the triggered release group (green) *vs.* the non-irradiated group (blue) reveals striking differences in toxicity. (B) Treatments with free nZnO (16.3 μg mL^{-1}), free PTX (40 nM) and free nZnO/PTX (16.3 μg mL^{-1}–40 nM) compared to Enc-nZnO/PTX (16.3 μg mL^{-1}–40 nM) for control comparison. Interestingly, there was a drastic improvement in the drug's efficacy in the triggered release group, most likely due to localized release of the drug in the vicinity of the cells.

It is possible that there could be synergistic effects from co-treatment with both nZnO and PTX in this cell line. As seen with the controls in Fig. 6B, the free nZnO had no effect on the viability profile, and the treatment with 40 nM free PTX had a somewhat similar effect to the non-triggered release Enc-nZnO/PTX group. Also, co-treatment with both the free nZnO and PTX led to no appreciable increase in toxicity, when compared to the PTX treatment alone.

We believe that this dramatic reduction in the viability of T47D cells is partly due to this cell line being adherent, whereas the Jurkat cells are a suspension cell line. The dispersion stability of nZnO most likely plays a role between these two cancer cell model systems. Previous reports on nZnO and other NPs revealed that over time, NPs settle to the bottom of the culture wells, affecting the dosimetry and cell viability.[27,42] Since the phototherapy was conducted 1.5 hours after nZnO

treatment, many of the particles likely settled to the bottom of the well before the irradiation occurred. Indeed, the confocal images of the Enc-nZnO treated T47D cells (Fig. 3) demonstrate a high accumulation of the encapsulated NPs in the local vicinity of the cells, further strengthening this thought. However, this alone cannot explain the differences in toxicity because the same nZnO was used in the control groups and due to the HDS differences, it would have settled to the bottom of the wells more quickly. It is likely that the encapsulation of PTX with nZnO brought a higher concentration of the drug to the local vicinity of the cells. In the free drug model, the drug is randomly distributed and can bind to hydrophobic pockets in serum proteins, preventing it from interacting with cells and reducing the overall toxicity. These results also support the concept that the localized release of the same overall drug concentration in the vicinity of cancerous cells can significantly improve the efficacy of the drug in the treatment of cancer. Lastly, the geometry of the two platforms potentially played a role. The Jurkat cells were cultured in 96-well plates with the media being deeper than the media in the 24-well plates used for the T47D cells. This extra depth likely caused more UV light to be absorbed, limiting interactions with Enc-nZnO/PTX and preventing full release of the nanoparticles and drug.

Discussion

These studies demonstrate that encapsulation of nZnO within a lipid carrier can effectively reduce and nearly eliminate its cytotoxic potential. Utilizing the inherent photocatalytic activity of nZnO allows for the controlled, on-demand release of the nanoparticles and chemotherapeutics utilizing UV light. The results obtained using the T47D breast cancer model were surprising and highlight the potential this approach may have in combating cancer while minimizing harm to cells in a non-irradiated location. However, for clinical applications, more progress is needed in the development of this system. For instance, the reason for the dramatic differences in viability profiles between the two models needs to be fully discerned. While there are a number of factors that were hypothesized to contribute to the differences (sedimentation of the particles, UV absorption in the media, and localized release of the drug), more research is needed to understand the differences and fully optimize this system to make it a viable treatment option.

While some factors, such as the lipid ratio and internal pH of the carrier, were investigated, optimization of other parameters and other potential applications need to be explored to maximize the capability of this system. Lipid encapsulation of nZnO is an effective approach to stabilize them in ionic solutions and it effectively eliminated the toxicity of nZnO in this system. Using the inherent ability of nZnO to induce ROS when irradiated, thus disrupting the capsule to release them and their contents, to our knowledge, has not been reported before. This strategy may further enhance the potential of inorganic NPs for use in therapeutics, and the ability to co-load both hydrophilic and hydrophobic drugs makes this a promising delivery platform for co-treatment strategies and for the treatment of various diseases.

Future work will evaluate modulating the composition of the nanoparticles to tailor their ROS production capabilities to different external stimuli. Using ultrasound is another feasible means to trigger the release from the carrier, as sonoexcitation of nZnO can induce ROS generation and could extend the use of this system to treat various diseases where photo-irradiation may be unadvisable. Other synthesis methods that produce different nanoparticle structures could further enhance this system, such as hollow nZnO spheres, in order to increase the drug-loading potential.[55] The versatility of a polymer coating will allow us to use targeting molecules, such as monoclonal antibodies and aptamers, conjugated to the surface of the lipid carrier. This could further enhance the localized concentration of the encapsulated NPs and chemotherapeutics. Other encapsulating materials, such as ROS-sensitive polymers and various other lipid compositions, will be evaluated to optimize this drug delivery platform. Since co-treatment with more than one chemotherapeutic drug is often utilized in the treatment of cancer, loading more than one drug with the carrier is achievable and may provide a new way of co-administering multiple drugs. Collectively, there are many avenues to pursue using this technology, which may extend its use to the treatment of various diseases beyond cancer.

Conclusion

ZnO nanomaterials have received considerable attention due to many promising attributes and there is an increasing number of applications being reported for the treatment of diseases. This paper demonstrates a new approach for utilizing the ROS-generating properties of nZnO and potentially other photocatalytic NPs for drug delivery. The lack of apparent toxicity of the encapsulated nZnO and the re-establishment of its anti-cancer activity in the triggered release groups are a step towards the goal of selectively treating cancer while preventing harm to normal cells. The extreme differences noted in the viability profiles of the T47D breast cancer cells treated with the co-encapsulated nZnO and PTX demonstrate the potential this system has for the co-delivery of multiple chemotherapeutics with on-demand release. Many parameters such as the encapsulation composition, conjugation of ligands, and making the particles stealth to the immune system, are just a few of the key features that need to be addressed, but there have been extensive studies reported with many novel methods to pursue. However, with the foundation laid, the aim of utilizing this system for the treatment of various diseases and specifically cancer appears feasible.

Methods

ZnO nanoparticle synthesis and characterization

All nZnO samples in this study were produced by a forced hydrolysis method that has been previously reported. Zinc acetate dihydrate and polyvinylpyrrolidone (PVP) were added

to diethylene glycol and heated to 80 °C at which point nanopure water was added, and then heated to and held at 150 °C for 75 minutes. After cooling to room temperature, the mixture was centrifuged at 41 140*g* and washed repeatedly with absolute ethanol. After the final wash and decantation, the pellet was dried overnight at 60 °C, pulverized with a mortar and pestle into a fine powder and subsequently annealed at 500 °C for 10 minutes.

nZnO was characterized by a variety of techniques including X-ray diffraction (XRD), transmission electron microscopy (TEM), Fourier transform infrared spectroscopy (FTIR), and X-ray photoelectron spectroscopy (XPS). A Rigaku Miniflex 600 XRD was used to verify the crystal phase and estimate the crystal size of nZnO. A JEOL JEM-2100 HR analytical TEM was used to verify the nZnO crystal size and visualize its morphology. To evaluate the sample purity, a Physical Electronics Versaprobe XPS system and a Bruker Tensor 27 spectrometer FTIR system were utilized. For FTIR experiments, the pellet method was used where 1.5 mg of the nZnO sample was ground with 0.200 g of spectroscopic grade KBr and subsequently pressed with 8 tons of pressure for 4 minutes. For dynamic light scattering and zeta potential measurements, 0.25 mg mL^{-1} of nZnO was suspended in nanopure water or in 130 mM NaCl and analyzed with a Malvern Zetasizer NanoZS.

Encapsulation of nZnO and cargo

nZnO was encapsulated in soy phosphatidylcholine (PC) and cholesterol (chol) at a 3 : 1 (w/w) ratio (Avanti Polar Lipids Inc., Alabaster, AL). The lipids and chol were dissolved in chloroform with a final concentration of 13.33 mg mL^{-1} (lipid + chol). The lipid/chol solution was then put under vacuum overnight to remove all solvent yielding a lipid/chol 'cake' and is referred to as "lipids". In the preparation of nZnO encapsulation, the following two steps were performed simultaneously: nZnO was suspended in 130 mM NaCl and sonicated for 45 minutes; 130 mM NaCl was added to the lipid cake for hydration and the solution was heated in a water bath to 60° C. Upon reaching 60 °C, the lipids were briefly sonicated and the nZnO solution was added to the lipid solution with a final nZnO concentration of 4.07 mg mL^{-1} (50 mM) in the following lipid to nZnO ratios: 3 : 4, 5 : 4, and 7 : 4 (w/w). The nZnO/lipid solution was then sonicated in a bath sonicator for 1 hour at 60 °C and stored at 4 °C until use. Encapsulation of the fluorescent dye 5(6)-carboxyfluorescein (CF) with nZnO followed the same procedure with the following modification: a solution comprised of 30 mM CF and 100 mM NaCl was utilized to prevent osmotic pressure artifacts when resuspending the lipid-coated particles in 130 mM NaCl. The CF/NaCl solution was adjusted to pH 7.4 and 9.85 by adding appropriate amounts of NaOH. For paclitaxel (PTX) loading, a 2 mM stock solution was first prepared by dissolving PTX (Alfa Aesar, Haverhill, MA) in DMSO. To co-encapsulate PTX with nZnO, an appropriate amount of the PTX stock solution was added to the lipid/chol mixture while in the chloroform solution and then all subsequent procedures were carried out as described above.

Simulated drug release

The fluorescent dye CF was utilized as a model for hydrophilic drug release and was co-loaded with nZnO as described. The dye was loaded at 30 mM, well above the self-quenching concentration (Fig. S4†) through the passive loading process. To remove CF from the exterior solution of the lipid capsule, the encapsulated nZnO/CF was repeatedly centrifuged at 296*g* for 2 minutes and the liquid was exchanged with a solution of 130 mM NaCl until the solution became clear. Fluorescence measurements were performed using a FluoroMax-4 spectrofluorometer with a working range of 285–750 nm. An excitation wavelength of 480 nm was used and emission spectra were collected from 490–600 nm. A self-quenching curve of CF was generated by performing fluorescence measurements with various concentrations of free CF in 130 mM NaCl to verify that the working concentrations were within the linear fluorescent region (Fig. S4†). Baseline measurements were first conducted ($F_{baseline}$) and then a 30 W, 365 nm LED lamp was used as a UV source to cause photoexcitation of nZnO and induce the triggered release of the fluorescent dye (F). To induce full release of the encapsulated dye (F_{total}), 20 μL of 5% Triton-X stock was then added to the solution. The percentage of released CF was determined using the following equation:

$$\%\ \text{released} = \frac{F - F_{baseline}}{(F_{total} - F_{baseline})} \times 100$$

Cell culture

To assess the cytotoxic effect of treatment with encapsulated nZnO (Enc-nZnO) and encapsulated nZnO with PTX (Enc-nZnO/PTX) on cancer cells, two human cell lines, acquired from the American Type Culture Collection (ATCC), were utilized: Jurkat (ATCC TIB-152), a suspension cell line derived from acute T cell leukemia, and T47D (ATCC HTB-133), an adherent cell line derived from ductal breast carcinoma (ATCC; Manassas, VA). Both cell lines were cultured in the log phase at 37 °C under 5% CO_2 using RPMI 1640 medium supplemented with 10% FBS (fetal bovine serum), 1% penicillin/streptomycin, 2 mM L-glutamine, and for T47D cells, 0.2 units per mL of bovine insulin following ATCC recommendations.

nZnO and live cell imaging

To evaluate the encapsulation efficiency of nZnO within a lipid membrane, imaging experiments were performed. The Enc-nZnO sample was transferred into a Nunc Lab-Tek II Chambered Coverglass 2 that contained 130 mM NaCl. Lipids were then stained with the plasma membrane stain Cell Mask Orange (CMO; Invitrogen, Carlsbad, CA) at a final concentration of 5 μg mL^{-1} for 30 minutes just prior to imaging.

A separate batch of encapsulated nZnO was made for electron microscopy imaging. The same procedure was utilized to encapsulate nZnO as before at a 5 : 4 lipid to ZnO ratio (w/w), with the only difference being that the solution was pure water instead of a 130 mM NaCl solution to prevent crystal formation during the drying procedure. After encapsulation, a 200 μL aliquot was placed into a 1 mL Eppendorf tube and frozen at

−80 °C. Once frozen, the sample was placed into a LabConco lyophilizer and lyophilized overnight. The resulting powder was sprinkled on a carbon-coated TEM grid. TEM images of the encapsulated nZnO were acquired with a JEOL JEM-2100 HR analytical TEM.

For live cell imaging of T47D breast cancer cells, the cells were transferred to a Nunc Lab-Tek II chamber in RPMI 1640 two days prior to imaging at a concentration of 100 000 cells per well and allowed to attach to the coverslip. After 24 hours, the medium was gently aspirated and then replaced with a custom-ordered HEPES-, phenol-, and phosphate-free RPMI 1640 (PPH-free RPMI 1640) (Thermo Fisher Scientific, Grand Island, NY). The media exchange was carried out to prevent the transformation and dissolution of nZnO induced by phosphate and HEPES, respectively.[56–58] Phenol red was also excluded to prevent fluorescence emissions during the imaging experiments. The cells were treated with Enc-nZnO 24 hours before imaging at a final concentration of 81.4 μg mL^{-1} (1 mM) for the non-triggered release experiments. In the triggered release group, the T47D cells were treated with a final nZnO concentration of 20.3 μg mL^{-1} (250 μM). CMO was added to the cultures and incubated for 30 minutes prior to imaging.

Confocal microscopy was used to image both Enc-nZnO and the T47D cells treated with Enc-nZnO. Images were acquired using a Zeiss 510 LSM system with the Zeiss Axiovert Observer Z1 inverted microscope and ZEN 2009 Imaging software (Carl Zeiss, Inc., Thornwood, NY) utilizing different objectives and band-pass filters. The nZnO used in this study was selected as it can be imaged directly using fluorescence microscopy techniques without causing modification to the nanoparticle. Using a configuration specific for the excitation and emission of the synthesized nZnO and CMO, images were collected with either a Plan-Apochromat 20×/NA 0.8 or a Plan-Apochromat oil 63×/NA 1.4 objective. The diode (405 nm) and HeNe (543 nm) lasers were used as excitation sources, and band-pass filters of 420–480 nm and 550–647 nm were used to image the nZnO and lipid layer, respectively.

Viability studies

For viability assessments, both Jurkat and T47D cells were cultured following ATCC recommendations as noted above. For the Jurkat T cell line, the cells were suspended in PPH-free RPMI 1640 and then seeded at a concentration of 2.5×10^5 cells per mL using the same media in a 96-well plate. For T47D cells, the cells were first seeded in the culture media at 1.0×10^5 cells per well in a 24-well plate a day prior to treatment to allow for cell attachment. The medium was then gently aspirated and replaced with the PPH free RPMI 1640 medium prior to treatment.

The Enc-nZnO and Enc-nZnO/PTX stocks were prepared, as indicated above, at a nZnO concentration of 4.07 mg mL^{-1} (50 mM) and pH = 7.2 to avoid potential effects on cell viability using a higher pH. For the free nZnO (non-encapsulated) controls, a fresh stock was prepared for each viability experiment by first suspending nZnO in nanopure water at a concentration of 4.07 mg mL^{-1} (50 mM) and sonicating for 20 minutes. The 2 mM PTX-DMSO solution was used to assess the free PTX effects on the cells as a control. Prior to treatment, the PTX-DMSO solution was added to fresh cellular media at the desired PTX concentration making the final DMSO concentration ≤0.2%. In the case of free nZnO, Enc-nZnO and Enc-nZnO/PTX, an appropriate amount of the stock solution was added to fresh cellular media to achieve a final nZnO concentration of 1.63 mg mL^{-1} (20 mM) prior to treatment in the well plates.

Once treated with nZnO, the cells were then cultured for 48 hours at 37 °C under 5% CO_2. For samples receiving UV irradiation, cultures were subjected to photo-irradiation 1.5 hours post nZnO treatment with the same excitation source utilized in the simulated drug release studies (30 W, 365 nm LED lamp). After optimizing the UV irradiation protocol for each cell line, it was determined that the required UV exposure was 3 minutes for Jurkat cells and 2 minutes for T47D cells to re-establish the toxicity of nZnO while minimizing the UV effects on the cell viability. The differences in optimized time of UV irradiation are likely due to the geometry of the culture plates. The 96-well plates containing the Jurkat cells had a deeper layer of media, likely limiting the depth penetration of UV irradiation due to absorption. Cell viability was assessed using the Alamar Blue metabolic assay. Alamar Blue was added to the wells at a final concentration of 10% 44 hours post-treatment and incubated for an additional 4 hours. The fluorescence intensity measurements were performed using a Biotek Synergy MX plate reader with excitation/emission wavelengths of 530/590 nm.

Abbreviations

nZnO	ZnO nanoparticles
NPs	Nanoparticles
ROS	Reactive oxygen species
PEG	Polyethylene glycol
EPR	Enhanced permeability and retention
DOPE	Dioleoylphosphatidylethanolamine
HDS	Hydrodynamic size
Enc-nZnO	Encapsulated ZnO nanoparticles
CF	5(6)-Carboxyfluorescein
PTX	Paclitaxel
Enc-nZnO/PTX	Co-encapsulated ZnO nanoparticles and paclitaxel

Data availability

All data supporting the findings of this study are available within the paper and its ESI.†

Conflicts of interest

There are no conflicts to declare.

Acknowledgements

This research was supported in part by NSF-MRI awards (#032233, #0722699 and #0521315) and the NIH (1R15CA141358-01). We also acknowledge support from the Institutional Development Awards (IDeA) from the National Institute of General Medical Sciences of the National Institutes of Health under Grants #P20GM103408, P20GM109095 and 1C06RR020533. We are thankful for the support from the Biomolecular Research Center at Boise State University, BSU-Biomolecular Research Center, RRID:SCR_019174, with funding from the National Science Foundation, Grants #0619793 and #0923535; the M. J. Murdock Charitable Trust; Lori and Duane Stueckle; and the Idaho State Board of Education.

References

1 D. Debela, S. Muzazu, K. Heraro, M. Ndalama, B. Mesele, D. Haile, S. Kitui and T. Manyazewal, *SAGE Open Med.*, 2021, **9**.
2 A. Yuzhalin, *Br. J. Cancer*, 2024, **130**, 1078–1082.
3 M. Lustberg, N. Kuderer, A. Desai, C. Bergerot and G. Lyman, *Nat. Rev. Clin. Oncol.*, 2023, **20**, 527–542.
4 D. Bobo, K. J. Robinson, J. Islam, K. J. Thurecht and S. R. Corrie, *Pharm. Res.*, 2016, **33**, 2373–2387.
5 M. Martinez-Carmona, Y. Gun'ko and M. Vallet-Regi, *Nanomaterials*, 2018, **8**, 27.
6 F. Muharnmad, M. Y. Guo, W. X. Qi, F. X. Sun, A. F. Wang, Y. J. Guo and G. S. Zhu, *J. Am. Chem. Soc.*, 2011, **133**, 8778–8781.
7 M. M. Khan, S. F. Adil and A. Al-Mayouf, *J. Saudi Chem. Soc.*, 2015, **19**, 462–464.
8 A. B. Djurisic, Y. H. Leung and A. M. C. Ng, *Mater. Horiz.*, 2014, **1**, 400–410.
9 J. Y. Li, D. D. Guo, X. M. Wang, H. P. Wang, H. Jiang and B. A. Chen, *Nanoscale Res. Lett.*, 2010, **5**, 1063–1071.
10 H. J. Zhang, Y. F. Shan and L. J. Dong, *J. Biomed. Nanotechnol.*, 2014, **10**, 1450–1457.
11 M. Ahmad, J. Zhao, J. Iqbal, W. Miao, L. Xie, R. Mo and J. Zhu, *J. Phys. D: Appl. Phys.*, 2009, **42**, 7.
12 Y. Li, J. F. Niu, W. Zhang, L. L. Zhang and E. X. Shang, *Langmuir*, 2014, **30**, 2852–2862.
13 Y. H. Leung, X. Y. Xu, A. P. Y. Ma, F. Z. Liu, A. M. C. Ng, Z. Y. Shen, L. A. Gethings, M. Y. Guo, A. B. Djurisic, P. K. H. Lee, H. K. Lee, W. K. Chan and F. C. C. Leung, *Sci. Rep.*, 2016, **6**, 13.
14 C. Mylonas and D. Kouretas, *In Vivo*, 1999, **13**, 295–309.
15 M. Premanathan, K. Karthikeyan, K. Jeyasubramanian and G. Manivannan, *Nanomedicine*, 2011, **7**, 184–192.
16 J. W. Rasmussen, E. Martinez, P. Louka and D. G. Wingettt, *Expert Opin. Drug Delivery*, 2010, **7**, 1063–1077.
17 M. J. Akhtar, M. Ahamed, S. Kumar, M. A. M. Khan, J. Ahmad and S. A. Alrokayan, *Int. J. Nanomed.*, 2012, **7**, 845–857.
18 C. Hanley, J. Layne, A. Punnoose, K. M. Reddy, I. Coombs, A. Coombs, K. Feris and D. Wingett, *Nanotechnology*, 2008, **19**, 10.
19 B. B. Manshian, S. Pokhrel, U. Himmelreich, K. Tamm, L. Sikk, A. Fernandez, R. Rallo, T. Tamm, L. Madler and S. J. Soenen, *Adv. Healthcare Mater.*, 2017, **6**, 11.
20 D. X. Ye, Y. Y. Ma, W. Zhao, H. M. Cao, J. L. Kong, H. M. Xiong and H. Mohwald, *ACS Nano*, 2016, **10**, 4294–4300.
21 B. Ghaemi, O. Mashinchian, T. Mousavi, R. Karimi, S. Kharrazi and A. Amani, *ACS Appl. Mater. Interfaces*, 2016, **8**, 3123–3134.
22 Y. Zhang, T. R. Nayak, H. Hong and W. Cai, *Curr. Mol. Med.*, 2013, **13**, 1633–1645.
23 I. A. Mudunkotuwa, T. Rupasinghe, C. M. Wu and V. H. Grassian, *Langmuir*, 2012, **28**, 396–403.
24 D. Cardoso, A. Narcy, S. Durosoy, C. Bordes and Y. Chevalier, *Powder Technol.*, 2021, **378**, 746–759.
25 T. Xia, M. Kovochich, M. Liong, L. Madler, B. Gilbert, H. B. Shi, J. I. Yeh, J. I. Zink and A. E. Nel, *ACS Nano*, 2008, **2**, 2121–2134.
26 Y. N. Chang, M. Y. Zhang, L. Xia, J. Zhang and G. M. Xing, *Materials*, 2012, **5**, 2850–2871.
27 C. B. Anders, J. J. Chess, D. G. Wingett and A. Punnoose, *Nanoscale Res. Lett.*, 2015, **10**, 22.
28 A. Abdelmonem, B. Pelaz, K. Kantner, N. Bigall, P. del Pino and W. Parak, *J. Inorg. Biochem.*, 2015, **153**, 334–338.
29 S. Raha and M. Ahmaruzzaman, *Nanoscale Adv.*, 2022, **4**, 1868–1925.
30 L. Sercombe, T. Veerati, F. Moheimani, S. Y. Wu, A. K. Sood and S. Hua, *Front. Pharmacol.*, 2015, **6**, 13.
31 B. S. Pattni, V. V. Chupin and V. P. Torchilin, *Chem. Rev.*, 2015, **115**, 10938–10966.
32 C. Zylberberg and S. Matosevic, *Drug Delivery*, 2016, **23**, 3319–3329.
33 G. T. Noble, J. F. Stefanick, J. D. Ashley, T. Kiziltepe and B. Bilgicer, *Trends Biotechnol.*, 2014, **32**, 32–45.
34 N. Bertrand, J. Wu, X. Y. Xu, N. Kamaly and O. C. Farokhzad, *Adv. Drug Delivery Rev.*, 2014, **66**, 2–25.
35 D. Rosenblum, N. Joshi, W. Tao, J. M. Karp and D. Peer, *Nat. Commun.*, 2018, **9**, 12.
36 H. Karanth and R. S. R. Murthy, *J. Pharm. Pharmacol.*, 2007, **59**, 469–483.
37 S. Simoes, J. N. Moreira, C. Fonseca, N. Duzgunes and M. C. P. de Lima, *Adv. Drug Delivery Rev.*, 2004, **56**, 947–965.
38 J. E. Eixenberger, C. B. Anders, K. Wada, K. M. Reddy, R. J. Brown, J. Moreno-Ramirez, A. E. Weltner, C. Karthik, D. A. Tenne, D. Fologea and D. G. Wingett, *ACS Appl. Mater. Interfaces*, 2019, **11**, 24933–24944.
39 A. Akbarzadeh, R. Rezaei-Sadabady, S. Davaran, S. W. Joo, N. Zarghami, Y. Hanifehpour, M. Samiei, M. Kouhi and K. Nejati-Koshki, *Nanoscale Res. Lett.*, 2013, **8**, 9.
40 Y. P. Patil and S. Jadhav, *Chem. Phys. Lipids*, 2014, **177**, 8–18.

41 S. W. Bian, I. A. Mudunkotuwa, T. Rupasinghe and V. H. Grassian, *Langmuir*, 2011, **27**, 6059–6068.
42 E. C. Cho, Q. Zhang and Y. N. Xia, *Nat. Nanotechnol.*, 2011, **6**, 385–391.
43 B. Dumontel, M. Canta, H. Engelke, A. Chiodoni, L. Racca, A. Ancona, T. Limongi, G. Canavese and V. Cauda, *J. Mater. Chem. B*, 2017, **5**, 8799–8813.
44 Q. B. Yang, T. S. Lin, C. Burton, S. H. Park and Y. F. Ma, *Toxicol. Res.*, 2016, **5**, 482–491.
45 E. Amstad, J. Kohlbrecher, E. Muller, T. Schweizer, M. Textor and E. Reimhult, *Nano Lett.*, 2011, **11**, 1664–1670.
46 S. L. Huang and R. C. MacDonald, *Biochim. Biophys. Acta, Biomembr.*, 2004, **1665**, 134–141.
47 H. L. Huang, P. H. Lu, H. C. Yang, G. D. Lee, H. R. Li and K. C. Liao, *Int. J. Nanomed.*, 2015, **10**, 5171–5185.
48 D. Y. Hegh, S. M. Mackay and E. W. Tan, *RSC Adv.*, 2014, **4**, 31771–31774.
49 A. Sandler, R. Gray, M. C. Perry, J. Brahmer, J. H. Schiller, A. Dowlati, R. Lilenbaum and D. H. Johnson, *N. Engl. J. Med.*, 2006, **355**, 2542–2550.
50 K. Miller, M. L. Wang, J. Gralow, M. Dickler, M. Cobleigh, E. A. Perez, T. Shenkier, D. Cella and N. E. Davidson, *N. Engl. J. Med.*, 2007, **357**, 2666–2676.
51 S. Koudelka and J. Turanek, *J. Controlled Release*, 2012, **163**, 322–334.
52 P. Ma and R. J. Mumper, *J. Nanomed. Nanotechnol.*, 2013, **4**, 16.
53 T. Yang, F. D. Cui, M. K. Choi, H. X. Lin, S. J. Chung, C. K. Shim and D. D. Kim, *Drug Delivery*, 2007, **14**, 301–308.
54 S. S. Hong, J. Y. Choi, J. O. Kim, M. K. Lee, S. H. Kim and S. J. Lim, *Int. J. Nanomed.*, 2016, **11**, 4465–4477.
55 N. Puvvada, S. Rajput, B. N. P. Kumar, S. Sarkar, S. Konar, K. R. Brunt, R. R. Rao, A. Mazumdar, S. K. Das, R. Basu, P. B. Fisher, M. Mandal and A. Pathak, *Sci. Rep.*, 2015, **5**, 15.
56 R. Herrmann, F. J. Garcia-Garcia and A. Reller, *Beilstein J. Nanotechnol.*, 2014, **5**, 2007–2015.
57 J. T. Lv, S. Z. Zhang, L. Luo, W. Han, J. Zhang, K. Yang and P. Christie, *Environ. Sci. Technol.*, 2012, **46**, 7215–7221.
58 J. E. Eixenberger, C. B. Anders, R. J. Hermann, R. J. Brown, K. M. Reddy, A. Punnoose and D. G. Wingett, *Chem. Res. Toxicol.*, 2017, **30**, 1641–1651.